Available online at www.sciencedirect.com
ScienceDirect
Journal of Sound and Vibration 306 (2007) 12–30
JOURNAL OF SOUND AND VIBRATION
www.elsevier.com/locate/jsvi

Free vibration analysis of rectangular plate with a hole by means of independent coordinate coupling method

Moon K. Kwak[a,*], Sangbo Han[b]

[a]Department of Mechanical Engineering, Dongguk University, 26 Pil-Dong 3-Ga, Joong-Gu, Seoul 100-715, Republic of Korea
[b]Department of Mechanical and Automation Engineering, Kyungnam University, 449 Wolyoung-Dong, Masan 631-701, Republic of Korea

Received 5 January 2007; received in revised form 22 May 2007; accepted 27 May 2007
Available online 2 July 2007

Abstract

This paper is concerned with the vibration analysis of a rectangular plate with a rectangular hole or a circular hole. In the previous researches, the effect of the hole is taken into account by subtracting the energies of the hole domain from the total energies of the whole plate. In doing so, the integrals of the functions consisting of the admissible functions based on the plate domain over hole domain lead to complex numerical computations. In this paper, a new methodology called Independent Coordinate Coupling Method (ICCM) was developed, in which the energies corresponding to the rectangular plate domain and the hole domain were derived independently and the two independent coordinates were coupled by imposing kinematic relations. By matching the deflection condition imposed on the expressions, the relationship between the global axes and the local axes can be easily derived and then used to construct the mass and stiffness matrices. The numerical results show the efficacy of the proposed method.

1. Introduction

A rectangular plate with a rectangular or a circular hole has been widely used as a substructure for ship, airplane, and plant. The vibration characteristics of a rectangular plate with a hole can be solved by either the Rayleigh–Ritz method (RRM) or the finite-element method. The RRM is an effective method when the rectangular plate has a rectangular hole. However, it cannot be easily applied to the case of a rectangular plate with a circular hole since the admissible functions for the rectangular hole domain do not permit closed-form integrals. The finite element method is a versatile tool for structural vibration analysis and therefore, can be applied to any of the cases mentioned above. But it does not permit qualitative analysis and requires enormous computational time.

Monahan et al. [1] applied the finite-element method to a clamped rectangular plate with a rectangular hole and verified the numerical results by experiments. Paramasivam [2] used the finite difference method for a simply-supported and clamped rectangular plate with a rectangular hole. Aksu and Ali [3] also used the finite difference method to analyze a rectangular plate with more than two holes. Rajamani and Prabhakaran [4]

*Corresponding author. Tel.: +82 2 2260 3705; fax: +82 2 2263 9379.
E-mail address: kwakm@dongguk.edu (M.K. Kwak).

0022-460X/$ - see front matter © 2007 Elsevier Ltd. All rights reserved.
doi:10.1016/j.jsv.2007.05.041

assumed that the effect of a hole is equivalent to an externally applied loading and carried out a numerical analysis based on this assumption for a composite plate. Rajamani and Prabhakaran [5] investigated the effect of a hole on the natural vibration characteristics of isotropic and orthotropic plates with simply-supported and clamped boundary conditions. Ali and Atwal [6] applied the RRM to a simply-supported rectangular plate with a rectangular hole, using the static deflection curves for a uniform loading as admissible functions. Lam et al. [7] divided the rectangular plate with a hole into several subareas and applied the modified RRM. Lam and Hung [8] applied the same method to a stiffened plate. The admissible functions used in Refs. [7,8] are the orthogonal polynomial functions proposed by Bhat [9–11]. Laura et al. [12] calculated the natural vibration characteristics of a simply-supported rectangular plate with a rectangular hole by the classical RRM. Sakiyama et al. [13] analyzed the natural vibration characteristics of an orthotropic plate with a square hole by means of the Green function assuming the hole as an extremely thin plate.

The vibration analysis of a rectangular plate with a circular hole does not lend an easy approach since the geometry of the hole is not the same as the geometry of the rectangular plate. Takahashi [14] used the classical RRM after deriving the total energy by subtracting the energy of the hole from the energy of the whole plate. He employed the eigenfunctions of a uniform beam as admissible functions. Joga-Rao and Pickett [15] proposed the use of algebraic polynomial functions and biharmonic singular functions. Kumai [16], Hegarty and Ariman [17], Eastep and Hemmig [18], and Nagaya [19] used the point-matching method for the analysis of a rectangular plate with a circular hole. The point-matching method employed the polar coordinate system based on the circular hole and the boundary conditions were satisfied along the points located on the sides of the rectangular plate. Lee and Kim [20] carried out vibration experiments on the rectangular plates with a hole in air and water. Kim et al. [21] performed the theoretical analysis on a stiffened rectangular plate with a hole.

In this study, we proposed a new method that can be effectively used for the analysis of a rectangular plate with either a circular or a rectangular hole. The new method is based on the classical RRM but utilizes different coordinate systems for the plate and the hole. In the RRM, the effect of the hole can be considered by the subtraction of the energy for the hole domain in deriving the total energy. In doing so, the previous researches considered only the global coordinate system for the integration. We proposed the use of the global coordinate system for the plate and the local coordinate system for the hole, separately. In this case, both the energy for the whole plate and the energy for the hole to be subtracted can be easily derived. Since different coordinate systems are used for the plate and the hole, we need a matching condition. The matching condition of deflections inside the hole domain provides the kinematic relation between the independent coordinate systems, and enables us to unify the two independent energies. We named this method the Independent Coordinate Coupling Method (ICCM). The advantage of the ICCM is that we do not need a complex integration process to obtain the total energy. In this paper, the ICCM was applied to the rectangular plate with a rectangular hole and the rectangular plate with a circular hole. The numerical results for the rectangular plates with the two types of holes, respectively, are compared to the numerical results of the classical approach, the finite-element method, and the experimental results. The numerical results show the efficacy of the proposed method.

2. RRM for free vibration analysis of rectangular plate

Let us consider a rectangular plate with side lengths a in the X direction and b in the Y direction as shown in Fig. 1. The kinetic and potential energies of the rectangular plate can be expressed as

$$T_P = \frac{1}{2}\rho h \int_0^a \int_0^b \dot{w}^2 \, \mathrm{d}x \, \mathrm{d}y, \tag{1}$$

$$V_P = \frac{1}{2} D \int_0^a \int_0^b \left[\left(\frac{\partial^2 w}{\partial x^2} \right)^2 + \left(\frac{\partial^2 w}{\partial y^2} \right)^2 + 2\nu \left(\frac{\partial^2 w}{\partial x^2} \frac{\partial^2 w}{\partial y^2} \right) + 2(1-\nu) \left(\frac{\partial^2 w}{\partial x \, \partial y} \right)^2 \right] \mathrm{d}x \, \mathrm{d}y, \tag{2}$$

where $w = w(x, y, t)$ represents the deflection of the plate, ρ the mass density, h the thickness, $D = Eh^3/12(1-\nu^2)$, E the Young's modulus, and ν the Poisson's ratio.

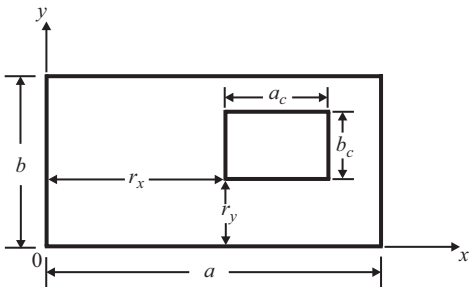

Fig. 1. Rectangular plate with a rectangular hole.

By using the non-dimensional variables, $\xi = x/a$, $\eta = y/b$ and the assumed mode method, the deflection of the plate can be expressed as

$$w(\xi, \eta, t) = \Phi(\xi, \eta) q(t), \tag{3}$$

where $\Phi(\xi, \eta) = [\Phi_1 \Phi_2 \dots \Phi_m]$ is a $1 \times m$ matrix consisting of the admissible functions and $q(t) = [q_1 q_2 \dots q_m]^{\mathrm{T}}$ is a $m \times 1$ vector consisting of generalized coordinates, in which m is the number of admissible functions used for the approximation of the deflection. Inserting Eq. (3) into Eqs. (1) and (2) results in Eq. (4):

$$T_P = \frac{1}{2} \dot{q}^{\mathrm{T}} M \dot{q}, \quad V_P = \frac{1}{2} q^{\mathrm{T}} K q, \tag{4a,b}$$

where

$$M = \rho h a b \, \bar{M}, \quad K = \frac{Db}{a^3} \bar{K}. \tag{5a,b}$$

In which

$$\bar{M} = \int_0^1 \int_0^1 \Phi^{\mathrm{T}} \Phi \, \mathrm{d}\xi \, \mathrm{d}\eta, \tag{6a}$$

$$\bar{K} = \int_0^1 \int_0^1 \left[\frac{\partial^2 \Phi^{\mathrm{T}}}{\partial \xi^2} \frac{\partial^2 \Phi}{\partial \xi^2} + \alpha^4 \frac{\partial^2 \Phi^{\mathrm{T}}}{\partial \eta^2} \frac{\partial^2 \Phi}{\partial \eta^2} + \nu \alpha^2 \left(\frac{\partial^2 \Phi^{\mathrm{T}}}{\partial \xi^2} \frac{\partial^2 \Phi}{\partial \eta^2} + \frac{\partial^2 \Phi^{\mathrm{T}}}{\partial \eta^2} \frac{\partial^2 \Phi}{\partial \xi^2} \right) + 2(1-\nu) \alpha^2 \frac{\partial^2 \Phi^{\mathrm{T}}}{\partial \xi \, \partial \eta} \frac{\partial^2 \Phi}{\partial \xi \partial \eta} \right] \mathrm{d}\xi \, \mathrm{d}\eta. \tag{6b}$$

$\bar{M}$, $\bar{K}$ represent the non-dimensionalized mass and stiffness matrices, respectively, and $\alpha = a/b$ represents the aspect ratio of the plate. The equation of motion can be derived by inserting Eq. (4) into the Lagrange's equation and the eigenvalue problem can be expressed as

$$[K - \omega^2 M] A = 0. \tag{7}$$

If we use the non-dimensionalized mass and stiffness matrices introduced in Eq. (5), the eigenvalue problem given by Eq. (7) can be also non-dimensionalized

$$[\bar{K} - \bar{\omega}^2 \bar{M}] A = 0, \tag{8}$$

where $\bar{\omega}$ is the non-dimensionalized natural frequency, which has the relationship with the natural frequency as follows:

$$\bar{\omega} = \omega \sqrt{\frac{\rho h a^4}{D}}. \tag{9}$$

To calculate the mass and stiffness matrices given by Eq. (6) easily, the admissible function matrix given by Eq. (3) needs to be expressed in terms of admissible function matrices in each direction.

$$\Phi_i(\xi, \eta) = \phi_i(\xi) \psi_i(\eta), \quad i = 1, 2, \dots, m \tag{10}$$

Then, the non-dimensionalized mass and stiffness matrices given by Eq. (6) can be expressed as

$$\bar{M}_{ij} = X_{ij} Y_{ij}, \tag{11a}$$

$$\bar{K}_{ij} = \hat{X}_{ij} Y_{ij} + \alpha^4 X_{ij} \hat{Y}_{ij} + \alpha^2 v\left(\tilde{X}_{ji} \tilde{Y}_{ij} + \tilde{X}_{ij} \tilde{Y}_{ji}\right) + \alpha^2 (1-v) \bar{X}_{ij} \bar{Y}_{ij}, \quad i,j = 1,2,\ldots,m, \tag{11b}$$

where

$$X_{ij} = \int_0^1 \phi_i \phi_j \, \mathrm{d}\xi, \quad \bar{X}_{ij} = \int_0^1 \phi_i' \phi_j' \, \mathrm{d}\xi, \quad \hat{X}_{ij} = \int_0^1 \phi_i'' \phi_j'' \, \mathrm{d}\xi, \quad \tilde{X}_{ij} = \int_0^1 \phi_i \phi_j'' \, \mathrm{d}\xi, \tag{12a-d}$$

$$Y_{ij} = \int_0^1 \psi_i \psi_j \, \mathrm{d}\eta, \quad \bar{Y}_{ij} = \int_0^1 \psi_i' \psi_j' \, \mathrm{d}\eta, \quad \hat{Y}_{ij} = \int_0^1 \psi_i'' \psi_j'' \, \mathrm{d}\eta, \quad \tilde{Y}_{ij} = \int_0^1 \psi_i \psi_j'' \, \mathrm{d}\eta, \quad i,j = 1,2,\ldots,m. \tag{12e-h}$$

If n admissible functions are used in the X and Y directions and the combination of admissible functions are used, a total of n^2 admissible functions can be obtained, which yields $m = n^2$. If each type of admissible functions are considered as $\chi_i (i = 1, 2, \ldots, n)$ and $\gamma_i (i = 1, 2, \ldots, n)$, then the relationship of between the sequence of the admissible function introduced in Eq. (10) and those of separated admissible functions can be expressed as

$$\phi_k = \begin{cases} \chi_1 & 1 \leqslant k \leqslant n \\ \chi_2 & n+1 \leqslant k \leqslant 2n \\ \chi_3 & 2n+1 \leqslant k \leqslant 3n \\ & \vdots \\ \chi_n & (n-1)n+1 \leqslant k \leqslant n^2 \end{cases}, \quad \psi_k = \begin{cases} \gamma_k & 1 \leqslant k \leqslant n \\ \gamma_{k-n} & n+1 \leqslant k \leqslant 2n \\ \gamma_{k-2n} & 2n+1 \leqslant k \leqslant 3n \\ & \vdots \\ \gamma_{k-(n-1)n} & (n-1)n+1 \leqslant k \leqslant n^2 \end{cases}. \tag{13a,b}$$

Therefore, instead of integrating $m^2 = n^4$ elements in Eq. (12), n^2 integrations and matrix rearrangement will suffice. First, let us calculate the following:

$$\Sigma_{ij} = \int_0^1 \chi_i \chi_j \, \mathrm{d}\xi, \quad \bar{\Sigma}_{ij} = \int_0^1 \chi_i' \chi_j' \, \mathrm{d}\xi, \quad \hat{\Sigma}_{ij} = \int_0^1 \chi_i'' \chi_j'' \, \mathrm{d}\xi, \quad \tilde{\Sigma}_{ij} = \int_0^1 \chi_i \chi_j'' \, \mathrm{d}\xi \tag{14a-d}$$

$$\Gamma_{ij} = \int_0^1 \gamma_i \gamma_j \, \mathrm{d}\eta, \quad \bar{\Gamma}_{ij} = \int_0^1 \gamma_i' \gamma_j' \, \mathrm{d}\eta, \quad \hat{\Gamma}_{ij} = \int_0^1 \gamma_i'' \gamma_j'' \, \mathrm{d}\eta, \quad \tilde{\Gamma}_{ij} = \int_0^1 \gamma_i \gamma_j'' \, \mathrm{d}\eta, \quad i,j = 1,2,\ldots,n. \tag{14e-h}$$

And then the matrices given by Eq. (12) can be derived as follows:

$$X = \begin{bmatrix} \Sigma_{11}\bar{I} & \Sigma_{12}\bar{I} & \cdots & \Sigma_{1n}\bar{I} \\ \Sigma_{21}\bar{I} & \Sigma_{22}\bar{I} & \cdots & \Sigma_{2n}\bar{I} \\ \vdots & \vdots & \ddots & \vdots \\ \Sigma_{n1}\bar{I} & \Sigma_{n2}\bar{I} & \cdots & \Sigma_{nn}\bar{I} \end{bmatrix}, \quad \bar{X} = \begin{bmatrix} \bar{\Sigma}_{11}\bar{I} & \bar{\Sigma}_{12}\bar{I} & \cdots & \bar{\Sigma}_{1n}\bar{I} \\ \bar{\Sigma}_{21}\bar{I} & \bar{\Sigma}_{22}\bar{I} & \cdots & \bar{\Sigma}_{2n}\bar{I} \\ \vdots & \vdots & \ddots & \vdots \\ \bar{\Sigma}_{n1}\bar{I} & \bar{\Sigma}_{n2}\bar{I} & \cdots & \bar{\Sigma}_{nn}\bar{I} \end{bmatrix}, \tag{15a,b}$$

$$\hat{X} = \begin{bmatrix} \hat{\Sigma}_{11}\bar{I} & \hat{\Sigma}_{12}\bar{I} & \cdots & \hat{\Sigma}_{1n}\bar{I} \\ \hat{\Sigma}_{21}\bar{I} & \hat{\Sigma}_{22}\bar{I} & \cdots & \hat{\Sigma}_{2n}\bar{I} \\ \vdots & \vdots & \ddots & \vdots \\ \hat{\Sigma}_{n1}\bar{I} & \hat{\Sigma}_{n2}\bar{I} & \cdots & \hat{\Sigma}_{nn}\bar{I} \end{bmatrix}, \quad \tilde{X} = \begin{bmatrix} \tilde{\Sigma}_{11}\bar{I} & \tilde{\Sigma}_{12}\bar{I} & \cdots & \tilde{\Sigma}_{1n}\bar{I} \\ \tilde{\Sigma}_{21}\bar{I} & \tilde{\Sigma}_{22}\bar{I} & \cdots & \tilde{\Sigma}_{2n}\bar{I} \\ \vdots & \vdots & \ddots & \vdots \\ \tilde{\Sigma}_{n1}\bar{I} & \tilde{\Sigma}_{n2}\bar{I} & \cdots & \tilde{\Sigma}_{nn}\bar{I} \end{bmatrix}, \tag{15c,d}$$

$$Y=\begin{bmatrix} \Gamma & \Gamma & \cdots & \Gamma \\ \Gamma & \Gamma & \cdots & \Gamma \\ \vdots & \vdots & \ddots & \vdots \\ \Gamma & \Gamma & \cdots & \Gamma \end{bmatrix},\quad \bar{Y}=\begin{bmatrix} \bar{\Gamma} & \bar{\Gamma} & \cdots & \bar{\Gamma} \\ \bar{\Gamma} & \bar{\Gamma} & \cdots & \bar{\Gamma} \\ \vdots & \vdots & \ddots & \vdots \\ \bar{\Gamma} & \bar{\Gamma} & \cdots & \bar{\Gamma} \end{bmatrix},\quad \hat{Y}=\begin{bmatrix} \hat{\Gamma} & \hat{\Gamma} & \cdots & \hat{\Gamma} \\ \hat{\Gamma} & \hat{\Gamma} & \cdots & \hat{\Gamma} \\ \vdots & \vdots & \ddots & \vdots \\ \hat{\Gamma} & \hat{\Gamma} & \cdots & \hat{\Gamma} \end{bmatrix},\quad \hat{Y}=\begin{bmatrix} \hat{\Gamma} & \hat{\Gamma} & \cdots & \hat{\Gamma} \\ \hat{\Gamma} & \hat{\Gamma} & \cdots & \hat{\Gamma} \\ \vdots & \vdots & \ddots & \vdots \\ \hat{\Gamma} & \hat{\Gamma} & \cdots & \hat{\Gamma} \end{bmatrix}, \tag{15e–h}$$

where $\bar{I}$ is an $n\times n$ matrix full of ones.

Let us consider the simply-supported case in the X direction. In this case, the eigenfunction of the uniform beam can be used as an admissible function.

$$\chi_i=\sqrt{2}\,\sin\, i\pi\xi,\quad i=1,2,\ldots n. \tag{16}$$

Inserting Eq. (16) into Eq. (14) yields

$$\Sigma_{ij}=\begin{cases}1, & i=j\\ 0, & i\neq j\end{cases},\quad \bar{\Sigma}_{ij}=\begin{cases}(i\pi)^2, & i=j\\ 0, & i\neq j\end{cases},\quad \hat{\Sigma}_{ij}=\begin{cases}(i\pi)^4, & i=j\\ 0, & i\neq j\end{cases},\quad \tilde{\Sigma}_{ij}=\begin{cases}-(i\pi)^2, & i=j,\\ 0, & i\neq j.\end{cases} \tag{17a–d}$$

In the case of the clamped condition in the X direction, the eigenfunction of a clamped–clamped uniform beam can be used:

$$\chi_i=\cosh\,\lambda_i\xi-\cos\,\lambda_i\xi-\sigma_i(\sinh\,\lambda_i\xi-\sin\,\lambda_i\xi),\quad i=1,2,\ldots,n, \tag{18}$$

where $\lambda_i=4.730,\ 7.853,\ 10.996,\ 14.137,\ldots$ and $\sigma_i=(\cosh\lambda_i-\cos\lambda_i)/(\sinh\lambda_i-\sin\lambda_i)$. Inserting Eq. (18) into Eq. (14) yields

$$\Sigma_{ij}=\begin{cases}1, & i=j,\\ 0, & i\neq j,\end{cases}$$

$$\bar{\Sigma}_{ij}=\begin{cases}\sigma_i\lambda_i(\sigma_i\lambda_i-2), & i=j,\\ 4\lambda_i^2\lambda_j^2(\sigma_j\lambda_j-\sigma_i\lambda_i)[1+(-1)^{i+j}]/(\lambda_i^4-\lambda_j^4), & i\neq j,\end{cases} \tag{19a, b}$$

$$\hat{\Sigma}_{ij}=\begin{cases}\lambda_i^4, & i=j,\\ 0, & i\neq j,\end{cases}$$

$$\hat{\Sigma}_{ij}=\begin{cases}\sigma_i\lambda_i(2-\sigma_i\lambda_i), & i=j,\\ 4\lambda_i^2\lambda_j^2(\sigma_i\lambda_i-\sigma_j\lambda_j)[1+(-1)^{i+j}]/(\lambda_i^4-\lambda_j^4), & i\neq j.\end{cases} \tag{19c, d}$$

In the case of a free-edge condition in the X direction, we can use the eigenfunction of a free–free uniform beam:

$$\chi_1=1,\quad \chi_2=\sqrt{12}\left(\xi-\frac{1}{2}\right), \tag{20a,b}$$

$$\chi_{i+2}=\cosh\,\lambda_i\xi+\cos\,\lambda_i\xi-\sigma_i(\sinh\,\lambda_i\xi+\sin\,\lambda_i\xi),\quad i=1,2,\ldots n-2, \tag{20c}$$

where λ_i and σ_i are the same as the ones for the clamped–clamped beam, and the first and the second modes represent the rigid-body modes. Inserting Eq. (20) into Eq. (14) yields Eq. (21).

$$\Sigma_{ij}=\begin{cases}1, & i=j\\ 0, & i\neq j\end{cases},\quad i=1,2,\ldots,n,\quad j=1,2,\ldots,n \tag{21a}$$

$$\bar{\Sigma}_{1j} = 0, \quad j = 1,2,\ldots,n,$$

$$\bar{\Sigma}_{2j} = \begin{cases} 0, & j = 1, \\ 12, & j = 2, \\ -2\sqrt{12}[1+(-1)^{j-2}], & j = 3,4,\ldots,n, \end{cases} \tag{21b,c}$$

$$\bar{\Sigma}_{(i+2)(j+2)} = \begin{cases} \sigma_i\lambda_i(\sigma_i\lambda_i+6), & i=j, \\ 4\lambda_i\lambda_j(\sigma_j\lambda_i^3-\sigma_i\lambda_j^3)[1+(-1)^{i+j}]/(\lambda_i^4-\lambda_j^4), & i\neq j, \end{cases}$$
$$i = 1,2,\ldots,n-2, \quad j = 1,2,\ldots,n-2, \tag{21d}$$

$$\hat{\Sigma}_{ij} = 0, \quad i = 1,2, \quad j = 1,2,\ldots,n, \tag{21e}$$

$$\hat{\Sigma}_{(i+2)(j+2)} = \begin{cases} \lambda_i^4, & i=j \\ 0, & i\neq j \end{cases}, \quad i = 1,2,\ldots,n-2, \quad j = 1,2,\ldots,n-2, \tag{21f}$$

$$\tilde{\Sigma}_{1j} = 0, \quad j = 1,2, \quad \tilde{\Sigma}_{(1)(j+2)} = 2\sigma_j\lambda_j[1-(-1)^j], \quad j = 1,2,\ldots,n-2, \tag{21g}$$

$$\tilde{\Sigma}_{2j} = 0, \quad j = 1,2, \quad \tilde{\Sigma}_{(2)(j+2)} = \sqrt{12}[1+(-1)^j](2-\sigma_j\lambda_j), \quad j = 1,2,\ldots,n-2, \tag{21h}$$

$$\tilde{\Sigma}_{(i+2)(j)} = 0, \quad i = 1,2,\ldots,n-2, \quad j = 1,2, \tag{21i}$$

$$\tilde{\Sigma}_{(i+2)(j+2)} = \begin{cases} \sigma_i\lambda_i(2-\sigma_i\lambda_i), & i=j, \\ 4\lambda_j^4(\sigma_i\lambda_i-\sigma_j\lambda_j)[1+(-1)^{i+j}]/(\lambda_i^4-\lambda_j^4), & i\neq j, \end{cases}$$
$$i = 1,2,\ldots,n-2, \quad j = 1,2,\ldots,n-2. \tag{21j}$$

For the admissible functions in the y direction, γ_i, the same method can be applied. The combination of different admissible functions can yield various boundary conditions.

3. Free vibration of circular plates

Let us consider a uniform circular plate with radius, R, and thickness, h. In this case, the kinetic and potential energies can be expressed as follows:

$$T_C = \frac{1}{2}\rho h\int_0^{2\pi}\int_0^R \dot{w}_c^2 r\,\mathrm{d}r\,\mathrm{d}\theta, \tag{22a}$$

$$V_C = \frac{1}{2}D\int_0^{2\pi}\int_0^R \left\{\left(\frac{\partial^2 w_c}{\partial r^2}+\frac{1}{r}\frac{\partial w_c}{\partial r}+\frac{1}{r^2}\frac{\partial^2 w_c}{\partial\theta^2}\right)^2 - 2(1-\nu)\left[\left(\frac{\partial^2 w_c}{\partial r^2}\right)\left(\frac{1}{r}\frac{\partial w_c}{\partial r}+\frac{1}{r^2}\frac{\partial^2 w_c}{\partial\theta^2}\right)\right.\right.$$
$$\left.\left. + -\left(\frac{1}{r}\frac{\partial^2 w_c}{\partial r\,\partial\theta}-\frac{1}{r^2}\frac{\partial^2 w_c}{\partial\theta^2}\right)^2\right]\right\} r\,\mathrm{d}r\,\mathrm{d}\theta. \tag{22b}$$

Unlike the uniform rectangular plate, simply-supported, clamped, and free-edge uniform circular plates have eigenfunctions. Hence, the deflection of the circular plate can be expressed as the combination of eigenfunctions and generalized coordinates

$$w_c(r,\theta,t) = \sum_{i=1}^{n_c}\Phi_{ci}(r,\theta)q_{ci}(t) = \Phi_c(r,\theta)q_c(t), \tag{23}$$

Table 1
Characteristic values for free-edge circular plate

k	n_k	λ_k	A_k	C_k	$f_k(\theta)$
1	2	2.3148	3.6459	0.2134	$\cos(2\theta)$
2	2	2.3148	3.6459	0.2134	$\sin(2\theta)$
3	0	3.0005	2.1979	−0.0857	1
4	3	3.5269	4.5155	0.0911	$\cos(3\theta)$
5	3	3.5269	4.5155	0.0911	$\sin(3\theta)$
6	1	4.5249	3.8349	−0.0192	$\cos(\theta)$
7	1	4.5249	3.8349	−0.0193	$\sin(\theta)$
8	2	5.9380	4.4258	−0.0056	$\cos(2\theta)$
9	2	5.9380	4.4258	−0.0056	$\sin(2\theta)$
10	0	6.2003	3.1390	0.0032	1

where $\Phi_{ci}(r, \theta)$ represents the eigenfunction of the uniform circular plate and $q_c(t)$ represents the generalized coordinate. Inserting Eq. (23) into Eq. (22) results in the following:

$$T_C = \frac{1}{2}\dot{q}_c^{\mathrm{T}} M_c \dot{q}_c, \quad V_C = \frac{1}{2} q_c^{\mathrm{T}} K_c q_c, \tag{24a,b}$$

where

$$M_c = \rho h \pi R^2 I, \quad K_c = \frac{\pi D}{R^2} \Lambda_c, \tag{25a,b}$$

in which I is an $n_c \times n_c$ identity matrix, Λ_c is an $n_c \times n_c$ diagonal matrix whose diagonals are ${\lambda_i}^4$. The eigenvalue has the expression, $\lambda^4 = \omega^2 \rho h r^4 / D$.

Since our study is concerned with either a rectangular or a circular hole, we consider only a free-edge circular plate [22]. If the eigenfunctions are rearranged in ascending order, we can have

$$\Phi_{c1} = 1, \quad \Phi_{c2} = \frac{r}{R}\cos\theta, \quad \Phi_{c3} = \frac{r}{R}\sin\theta, \tag{26a−c}$$

$$\Phi_{c(k+3)} = A_k \left[J_{n_k}\left(\lambda_k \frac{r}{R}\right) + C_k I_{n_k}\left(\lambda_k \frac{r}{R}\right) \right] f_k(\theta), \quad k = 1, 2, \ldots, \tag{26d}$$

where J_{n_k} and I_{n_k} are the Bessel functions of the first kind and the modified Bessel functions of order n_k, respectively. The first three modes represent the rigid-body modes and other modes represent the elastic vibration modes. The characteristic values obtained from Eq. (26d) are tabulated in Table 1, and are listed by rearranging the values given in Ref. [22]. In this case, Λ_c has the following form:

$$\Lambda_c = \mathrm{diag}([0 \quad 0 \quad 0 \quad \lambda_1^4 \quad \lambda_2^4 \quad \lambda_3^4 \quad \ldots \quad \lambda_{n_c-3}^4]). \tag{27}$$

4. Free vibration analysis of a rectangular plate with a hole by use of global coordinates

Let us consider a rectangular plate with a rectangular hole, as shown in Fig. 1. In this case, the total kinetic and potential energies can be obtained by subtracting the energies belonging to the hole domain from the total energies for the global domain

$$T_{\mathrm{total}} = T_P - T_H = \frac{1}{2}\dot{q}^{\mathrm{T}}(M - M_H)\dot{q},$$
$$V_{\mathrm{total}} = V_P - V_H = \frac{1}{2} q^T (K - K_H) q, \tag{28a, b}$$

M_H, K_H reflect the reductions in mass and stiffness matrices and can be also expressed by non-dimensionalized mass and stiffness matrices, respectively,

$$M_H = \rho h a b \bar{M}_H, \quad K_H = \frac{Db}{a^3} \bar{K}_H, \tag{29a,b}$$

where

$$\bar{M}_H = \int_{\bar{r}_x}^{\bar{r}_x+\bar{a}_c} \int_{\bar{r}_y}^{\bar{r}_y+\bar{b}_c} \Phi^T \Phi \, \mathrm{d}\xi \, \mathrm{d}\eta, \tag{30a}$$

$$\bar{K}_H = \int_{\bar{r}_x}^{\bar{r}_x+\bar{a}_c} \int_{\bar{r}_y}^{\bar{r}_y+\bar{b}_c} \left[\frac{\partial^2 \Phi^{\mathrm{T}}}{\partial \xi^2} \frac{\partial^2 \Phi}{\partial \xi^2} + \alpha^4 \frac{\partial^2 \Phi^{\mathrm{T}}}{\partial \eta^2} \frac{\partial^2 \Phi}{\partial \eta^2} + \nu\alpha^2 \left(\frac{\partial^2 \Phi^{\mathrm{T}}}{\partial \xi^2} \frac{\partial^2 \Phi}{\partial \eta^2} + \frac{\partial^2 \Phi^{\mathrm{T}}}{\partial \eta^2} \frac{\partial^2 \Phi}{\partial \xi^2} \right) + 2(1-\nu)\alpha^2 \frac{\partial^2 \Phi^{\mathrm{T}}}{\partial \xi \, \partial \eta} \frac{\partial^2 \Phi}{\partial \xi \, \partial \eta} \right] \mathrm{d}\xi \, \mathrm{d}\eta \tag{30b}$$

in which $\bar{r}_x = r_x/a$, $\bar{r}_y = r_y/b$, $\bar{a}_c = a_c/a$, $\bar{b}_c = b_c/b$ represent various aspect ratios. Hence, the non-dimensionalized eigenvalue problem for the addressed problem can be expressed as

$$[(\bar{K} - \bar{K}_H) - \bar{\omega}^2(\bar{M} - \bar{M}_H)]A = 0. \tag{31}$$

To calculate the non-dimensionalized mass and stiffness matrices for the hole domain given by Eq. (30), we generally resort to numerical integration. However, in the case of a simply-supported rectangular plate with a rectangular hole, the exact expressions can be derived for the non-dimensionalized mass and stiffness matrices for the hole. If the admissible functions given by Eqs. (16) and (14) are used, the following expression for the components can be obtained, which are necessary for the calculation of the mass and stiffness matrices

$$(\Sigma_H)_{ij} = \begin{cases} \bar{a}_c - \delta_1, & i = j, \\ \delta_2 - \delta_3, & i \neq j, \end{cases} \quad (\bar{\Sigma}_H)_{ij} = \begin{cases} i^2\pi^2(\bar{a}_c + \delta_1), & i = j, \\ ij\pi^2(\delta_2 + \delta_3), & i \neq j, \end{cases} \tag{32a,b}$$

$$(\hat{\Sigma}_H)_{ij} = \begin{cases} i^4\pi^4(\bar{a}_c - \delta_1), & i = j, \\ i^2j^2\pi^4(\delta_2 - \delta_3), & i \neq j, \end{cases} \quad (\tilde{\Sigma}_H)_{ij} = \begin{cases} -i^2\pi^2(\bar{a}_c - \delta_1), & i = j, \\ -j^2\pi^2(\delta_2 - \delta_3), & i \neq j, \end{cases} \tag{32c,d}$$

where

$$\delta_1 = \frac{\sin 2i\pi(\bar{r}_x + \bar{a}_c) - \sin 2i\pi\bar{r}_x}{2i\pi}, \quad \delta_2 = \frac{\sin(i-j)\pi(\bar{r}_x + \bar{a}_c) - \sin(i-j)\pi\bar{r}_x}{(i-j)\pi}, \tag{33a,b}$$

$$\delta_3 = \frac{\sin(i+j)\pi(\bar{r}_x + \bar{a}_c) - \sin(i+j)\pi\bar{r}_x}{(i+j)\pi}. \tag{33c}$$

In the case of a clamped rectangular plate with a rectangular hole, the exact expressions can be derived for the components as in the case of the simply-supported rectangular plate with a rectangular hole. But the expressions are too complicated to be noted here. To avoid the lengthy expressions, we would rather resort to a numerical integration technique. However, the computational time becomes a concern when numerical integration is to be used. In the case of a circular hole, the exact expressions do not exist, so we must resort to numerical integration. To reduce the computational time due to numerical integration and to simplify the computation, a new method is developed in this study, which will be explained in the next section.

5. ICCM for a rectangular plate with a rectangular hole

Let us consider again the rectangular plate with a rectangular hole, as shown in Fig. 2. As can be seen from Fig. 2, the local coordinates fixed to the hole domain is introduced. Considering the non-dimensionalized coordinates, $\xi_h = x_c/a_c$, $\eta_h = y_c/b_c$, we can express the displacement inside the hole domain as

$$w_h(\xi_h, \eta_h) = \Phi_h(\xi_h, \eta_h) q_h, \tag{34}$$

where $\Phi_h(\xi_h, \eta_h) = [\Phi_{h1}\Phi_{h2} \ldots \Phi_{hm_h}]$ is the $1 \times m_h$ admissible function matrix, and $q_h(t) = [q_{h1}q_{h2} \ldots q_{hm_h}]^{\mathrm{T}}$ is the $m_h \times 1$ generalized coordinate vector. If we apply the separation of variables to the admissible function as

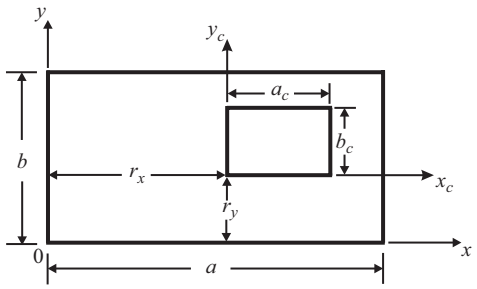

Fig. 2. Rectangular plate with a rectangular hole with local axes.

we did in Eq. (10), then we have

$$\Phi_{hi}(\xi_h,\eta_h)=\phi_{hi}(\xi_h)\psi_{hi}(\eta_h),\quad i=1,2,\ldots,m_h. \tag{35}$$

Using Eqs. (34) and (35), we can express the kinetic and potential energies in the hole domain as

$$T_H=\frac{1}{2}\,\dot{q}_h^{\mathrm{T}}M_h\dot{q}_h,\quad V_H=\frac{1}{2}\,q_h^{\mathrm{T}}K_hq_h. \tag{36a,b}$$

Hence, the total kinetic and potential energies can be written as

$$T_{\text{total}}=\frac{1}{2}\,\dot{q}^{\mathrm{T}}M\dot{q}-\frac{1}{2}\,\dot{q}_h^{\mathrm{T}}M_h\dot{q}_h,\quad V_{\text{total}}=\frac{1}{2}\,q^{\mathrm{T}}Kq-\frac{1}{2}\,q_h^{\mathrm{T}}K_hq_h, \tag{37a,b}$$

where

$$M_h=\rho ha_cb_c\bar{M}_h,\quad K_h=\frac{Db_c}{a_c^3}\,\bar{K}_h \tag{38a,b}$$

in which

$$\bar{M}_h=\int_0^1\int_0^1\Phi_h^{\mathrm{T}}\Phi_h\xi_h\,\mathrm{d}\eta_h, \tag{39a}$$

$$\begin{aligned}\bar{K}_h=\int_0^1\int_0^1\Bigg[&\frac{\partial^2\Phi_h^{\mathrm{T}}}{\partial\xi_h^2}\frac{\partial^2\Phi_h}{\partial\xi_h^2}+\alpha_c^4\frac{\partial^2\Phi_h^{\mathrm{T}}}{\partial\eta_h^2}\frac{\partial^2\Phi_h}{\partial\eta_h^2}+\nu\alpha_c^2\left(\frac{\partial^2\Phi_h^{\mathrm{T}}}{\partial\xi_h^2}\frac{\partial^2\Phi_h}{\partial\eta_h^2}+\frac{\partial^2\Phi_h^{\mathrm{T}}}{\partial\eta_h^2}\frac{\partial^2\Phi_h}{\partial\xi_h^2}\right)\\&+2(1-\nu)\alpha_c^2\frac{\partial^2\Phi_h^{\mathrm{T}}}{\partial\xi_h\partial\eta_h}\frac{\partial^2\Phi_h}{\partial\xi_h\partial\eta_h}\Bigg]\mathrm{d}\xi_h\,\mathrm{d}\eta_h\end{aligned} \tag{39b}$$

and $\alpha_c=a_c/b_c$. Note that the definite integrals in Eq. (39) has distinctive advantage compared to Eq. (30) because it has an integral limit from 0 to 1 thus permitting closed-form expressions. Therefore, we can use the same expression, Eq. (21), used for the free-edge rectangular plate.

Since the local coordinate system is used for the hole domain, we do not have to carry out integration, as in Eq. (30). However, the displacement matching condition between the global and local coordinates should be satisfied inside the hole domain. The displacement matching condition inside the hole domain can be written as

$$w_h(\xi_h,\eta_h)=w(\xi,\eta). \tag{40}$$

The relationship between the non-dimensionalized global and local coordinates can be written as

$$\xi=\frac{r_x}{a}+\frac{a_c}{a}\,\xi_h,\quad \eta=\frac{r_y}{b}+\frac{b_c}{b}\,\eta_h. \tag{41}$$

Considering Eqs. (3), (10), (34) and (35), and inserting them into Eq. (40), we can derive

$$\sum_{j=1}^{m_h}\Phi_{hj}(\xi_h,\eta_h)q_{hj}(t)=\sum_{j=1}^{m_h}\phi_{hj}(\xi_h)\psi_{hj}(\eta_h)q_{hj}(t)=\sum_{k=1}^{m}\Phi_k(\xi,\eta)q_k(t)=\sum_{k=1}^{m}\phi_k(\xi)\psi_k(\eta)q_k(t). \tag{42}$$

Multiplying Eq. (42) by $\phi_{hi}(\xi_h)\psi_{hi}(\eta_h)$ and performing integration, we can derive

$$\sum_{j=1}^{m_h}\int_0^1\int_0^1 \phi_{hi}(\xi_h)\psi_{hi}(\eta_h)\phi_{hj}(\xi_h)\psi_{hj}(\eta_h)\,\mathrm{d}\xi_h\,\mathrm{d}\eta_h\,q_{hj}(t)$$
$$=\sum_{k=1}^{m}\int_0^1\int_0^1 \phi_{hi}(\xi_h)\psi_{hi}(\eta_h)\phi_k(\xi)\psi_k(\eta)\,\mathrm{d}\xi_h\,\mathrm{d}\eta_h q_k(t),\quad i=1,2,\ldots,m_h. \tag{43}$$

Using the orthogonal property of the eigenfunctions of the uniform beam, Eq. (43) can be rewritten as

$$q_{hi}(t)=\sum_{k=1}^{m}\int_0^1 \phi_{hi}(\xi_h)\phi_k(\xi)\,\mathrm{d}\xi_h\int_0^1 \psi_{hi}(\eta_h)\psi_k(\eta)\,\mathrm{d}\eta_h q_k(t)$$
$$=\sum_{k=1}^{m}(T_h)_{ik}q_k(t),\quad i=1,2,\ldots,m_h. \tag{44}$$

If we express Eq. (44) in the matrix form, we can have

$$q_h=T_h q, \tag{45}$$

where T_h is the $m_h\times m$ transformation matrix between two coordinates. Inserting Eq. (45) into Eq. (37), we can derive

$$T_{\text{total}}=\frac{1}{2}\,\dot{q}^{\mathrm{T}}M\dot{q}-\frac{1}{2}\,\dot{q}^{\mathrm{T}}T_h^{\mathrm{T}}M_hT_h\dot{q}=\frac{1}{2}\,\dot{q}^{\mathrm{T}}M_r\dot{q}, \tag{46a}$$

$$V_{\text{total}}=\frac{1}{2}\,q^{\mathrm{T}}Kq-\frac{1}{2}\,q^{\mathrm{T}}T_h^{\mathrm{T}}K_hT_hq=\frac{1}{2}\,q^{\mathrm{T}}K_rq, \tag{46b}$$

where

$$M_r=M-T_h^{\mathrm{T}}M_hT_h,\quad K_r=K-T_h^{\mathrm{T}}K_hT_h. \tag{47a,b}$$

Eq. (47) can be expressed by means of non-dimensionalized parameters

$$M_r=\rho hab\bar{M}_r,\quad K_r=\frac{Db}{a^3}\,\bar{K}_r, \tag{48a,b}$$

where

$$\bar{M}_r=\bar{M}-(\bar{a}_c\bar{b}_c)T_h^{\mathrm{T}}\bar{M}_hT_h,\quad \bar{K}_r=\bar{K}-\frac{\bar{b}_c}{\bar{a}_c^3}\,T_h^{\mathrm{T}}\bar{K}_hT_h. \tag{49a,b}$$

Hence, the non-dimensionalized eigenvalue problem can be expressed as

$$[\bar{K}_r-\bar{\omega}^2\bar{M}_r]A=0. \tag{50}$$

In deriving the mass and stiffness matrices, Eq. (49), for the eigenvalue problem, we only needed the transformation matrix, T_h. $\bar{M}$, $\bar{K}$ can be easily computed by Eq. (11) according to the edge boundary conditions and $\bar{M}$, $\bar{K}$ can be computed from the results of Eq. (11) for the all free-edge rectangular plate. Compared to the approach based on the global coordinates, the numerical integration for the transformation matrix, T_h, is easy because of the integral limits. The process represented by Eqs. (45) and (49) is referred to as the ICCM in this study. The ICCM enables us to solve the free vibration problem of the rectangular plate with a rectangular hole more easily than the previous approaches do. The advantage of the ICCM becomes more apparent when we deal with a circular hole, as will be demonstrated in the next section.

6. ICCM for a rectangular plate with a circular hole

Let us consider a rectangular plate with a circular hole, as shown in Fig. 3. The total kinetic and potential energies of the rectangular plate with a circular hole are obtained by subtracting the energies of the circular hole domain from the energies of the whole plate, as we did for the case of a rectangular hole. Hence, the

following equations can be obtained by using Eqs. (4) and (24)

$$T_{\text{total}} = \frac{1}{2}\dot{q}^{\mathrm{T}} M \dot{q} - \frac{1}{2}\dot{q}_c^{\mathrm{T}} M_c \dot{q}_c, \quad V_{\text{total}} = \frac{1}{2} q^{\mathrm{T}} K q - \frac{1}{2} q_c^{\mathrm{T}} K_c q_c. \tag{51a,b}$$

In order to apply the ICCM, the displacement matching condition should be satisfied. Hence, the following condition should be satisfied inside the circular hole domain

$$w_c(r,\ \theta) = w(\xi, \eta). \tag{52}$$

Considering Eqs. (23), (3) and (10), we can obtain

$$\sum_{j=1}^{m_c} \Phi_{cj}(r,\theta) q_{cj}(t) = \sum_{k=1}^{m} \Phi_k(\xi,\eta) q_k(t) = \sum_{k=1}^{m} \phi_k(\xi)\psi_k(\eta) q_k(t). \tag{53}$$

Multiplying Eq. (53) by $\Phi_{ci}(r,\ \theta)$ and performing integration over the circular hole domain result in

$$\sum_{j=1}^{m_c} \int_0^{2\pi}\int_0^R \Phi_{ci}(r,\theta)\Phi_{cj}(r,\theta) r\,\mathrm{d}r\,\mathrm{d}\theta q_{cj}(t) = \sum_{k=1}^{m} \int_0^{2\pi}\int_0^R \Phi_{ci}(r,\theta)\phi_k(\xi)\psi_k(\eta) r\,\mathrm{d}r\,\mathrm{d}\theta q_k(t), \quad i = 1,2,\ldots,m. \tag{54}$$

Using the orthogonal property of $\Phi_{ci}(r,\ \theta)$, Eq. (54) can be rewritten as

$$q_{ci}(t) = \sum_{k=1}^{m} \int_0^{2\pi}\int_0^R \Phi_{ci}(r,\theta)\phi_k(\xi)\psi_k(\eta) r\,\mathrm{d}r\,\mathrm{d}\theta q_k(t) = \sum_{k=1}^{m} (T_c)_{ik} q_k(t), \quad i = 1,2,\ldots,m_c. \tag{55}$$

Eq. (55) can be expressed in matrix form:

$$q_c = T_c q, \tag{56}$$

where T_c is a $m_c \times m$ transformation matrix. We also need the relationship between the global and local coordinates, which can be expressed as follows:

$$\xi = \frac{r_x}{a} + \frac{r\cos\theta}{a}, \quad \eta = \frac{r_y}{b} + \frac{r\sin\theta}{b}. \tag{57}$$

Inserting Eqs. (51) and (56), we can express the total kinetic and potential energies as

$$T_{\text{total}} = \frac{1}{2}\dot{q}^{\mathrm{T}} M \dot{q} - \frac{1}{2}\dot{q}^{\mathrm{T}} T_c^{\mathrm{T}} M_c T_c \dot{q} = \frac{1}{2}\dot{q}^{\mathrm{T}} M_{cr} \dot{q}, \tag{58a}$$

$$V_{\text{total}} = \frac{1}{2} q^{\mathrm{T}} K q - \frac{1}{2} q^{\mathrm{T}} T_c^{\mathrm{T}} K_c T_c q = \frac{1}{2} q^{\mathrm{T}} K_{cr} q, \tag{58b}$$

where

$$M_{cr} = M - T_c^{\mathrm{T}} M_c T_c, \quad K_{cr} = K - T_c^{\mathrm{T}} K_c T_c. \tag{59a,b}$$

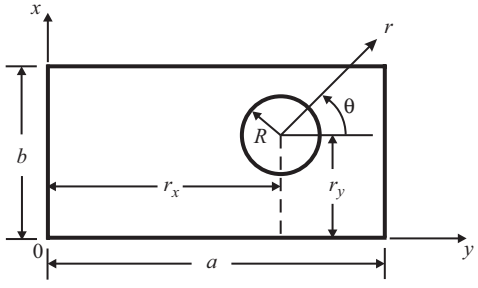

Fig. 3. Rectangular plate with a circular hole.

Eq. (59) can be non-dimensionalized using Eqs. (5) and (25) as for the rectangular hole. Hence, we obtain

$$M_{cr} = \rho hab\bar{M}_{cr}, \quad K_{cr} = \frac{Db}{a^3}\bar{K}_{cr}, \tag{60a,b}$$

where

$$\bar{M}_{cr} = \bar{M} - (\pi\alpha\beta^2)T_c^{\mathrm{T}}T_c, \quad \bar{K}_{cr} = \bar{K} - \left(\frac{\pi\alpha}{\beta^2}\right)T_c^{\mathrm{T}}\Lambda_c T_c \tag{61a,b}$$

in which $\beta = R/a$.

Therefore, the non-dimensionalized eigenvalue problem for the rectangular plate with a circular hole can be expressed as

$$[\bar{K}_{cr} - \bar{\omega}^2\bar{M}_{cr}]A = 0. \tag{62}$$

As shown in the process from Eqs. (56), (59) and (61), it can be readily seen that the application of the ICCM is very straightforward and the theoretical background is solid. The efficacy of the ICCM will be fully demonstrated in the next numerical results.

7. Numerical results

For the numerical calculation, $v = 0.3$ was considered for all cases. First, the effect of the number of admissible function on convergence was investigated by using the classical RRM for a simply-supported square plate with a square hole. Two holes of sizes $\bar{a}_c = 0.25$ and $= 0.5$ were considered. Errors were calculated based on the reference case, in which the total number of admissible functions was 400, which implies a combination of 20 admissible functions in each direction. Figs. 4 and 5 show that the errors of 5 natural frequencies converge to less than 5% if the number of admissible functions is greater than 100. The reason why the error of 2nd and 3rd modes is larger than others seems that the 2nd and 3rd modes have a diagonal nodal line so that admissible functions considered in this study do not render a good approximation for the 2nd and 3rd modes. Based on the numerical results, all numerical calculations followed were carried out by using 100 admissible functions, which implies 10 admissible functions in each direction. The next question arose regarding the optimal number of admissible functions for a rectangular hole domain when applying the ICCM. To this end, a simply-supported square plate with a square hole of dimension $\bar{a}_c = 0.25$

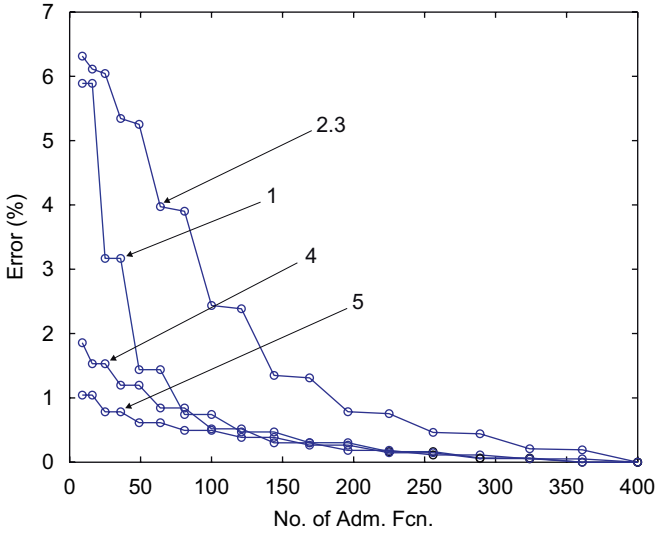

Fig. 4. Number of admissible functions vs. error for $\bar{a}_c = 0.25$.

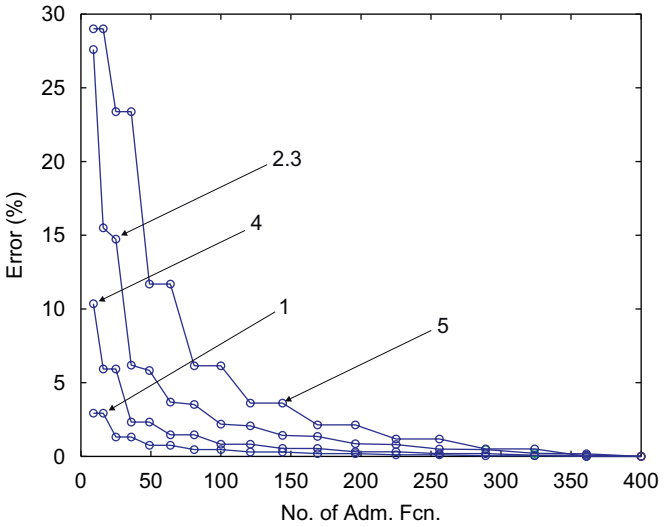

Fig. 5. Number of admissible functions vs. error for $\bar{a}_c = 0.5$.

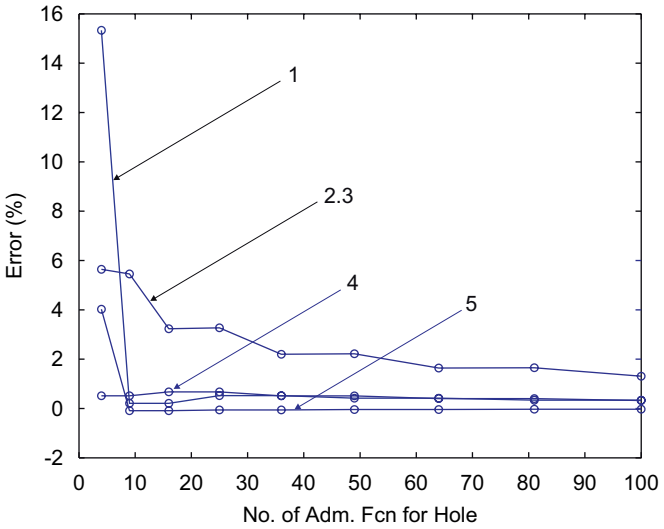

Fig. 6. Number of admissible functions for hole vs. error for $\bar{a}_c = 0.25$.

was considered, and the errors were calculated based on the result obtained by the classical RRM with 100 admissible functions. As shown in Fig. 6, the number of admissible functions greater than 25 for a rectangular hole domain can give less than 5% error. However, 100 admissible functions were used for the square hole domain when applying the ICCM to the simply-supported square plate with a square hole. The ICCM gave very good convergence. Figs. 7 and 8 show the non-dimensionalized frequencies for the simply-supported and clamped square plates with a square hole calculated by the classical RRM and the ICCM. As can be seen from Figs. 7 and 8, the results obtained by the ICCM are in good agreement with the results obtained by the classical RRM; this agreement proves the efficacy of the ICCM. To prove the computational efficiency of the ICCM, we computed the CPU times to complete the eigenvalue and eigenvector calculations and then compared the CPU time of the ICCM to the CPU time of the classical RRM. The computations were carried out on the AMD Athlon 64×2 dual core processor and the programs were written using Matlab. The Matlab quad function was used for the numerical integration. Fig. 9 shows the CPU times versus the square hole size

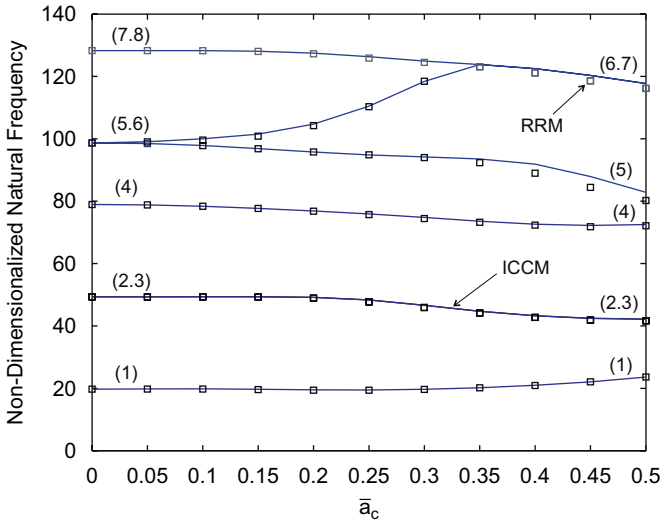

Fig. 7. Non-dimensionalized natural frequency vs. size of hole for simply-supported plate.

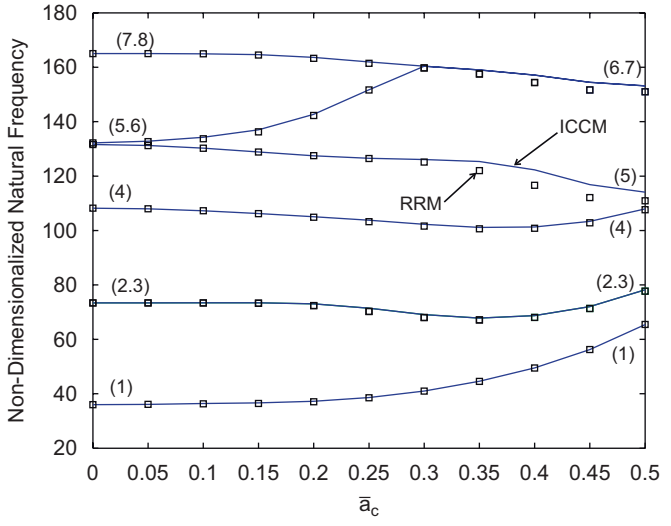

Fig. 8. Non-dimensionalized natural frequency vs. size of hole for clamped plate.

in the case of clamped square plate. As the hole size increases, the computational time in the classical RRM rapidly increases but the computational time in the ICCM stays in approximately 1 s, which proves the computational efficiency of the ICCM.

We carried out experiments on free-edge square aluminum plates with square and circular holes. Fig. 10 shows the theoretical results obtained by the ICCM and the experimental results. Fig. 10 shows that the results obtained by the ICCM are in good agreement with the experimental results. Fig. 11 shows the mode shapes of a simply-supported square plate with a square hole when $\bar{a}_c = 0.2$.

Figs. 12–14 show the non-dimensionalized frequencies of the simply-supported, clamped, and free-edge square plate with a circular hole. Since the case of the rectangular plate with a circular hole cannot be easily tackled by the classical RRM, we used a commercial finite element program such as ANSYS for comparison. Fig. 12 shows the comparison of the ICCM results to ANSYS results. It can be readily seen from Fig. 12 that the ICCM results are in good agreement with the ANSYS results. Fig. 14 shows that the results obtained by

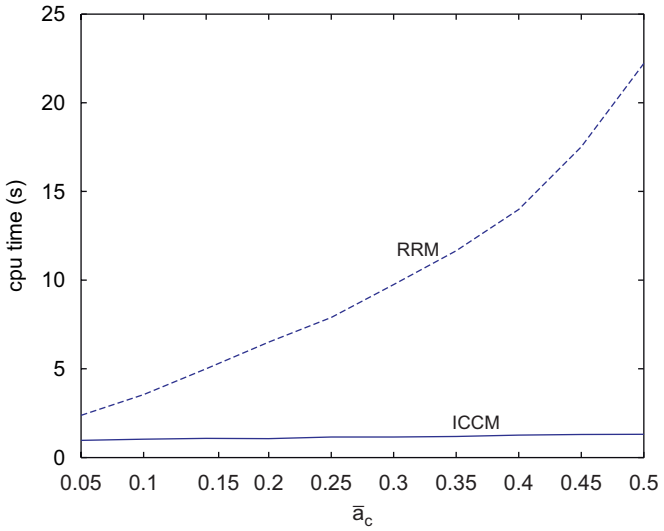

Fig. 9. CPU time comparison of classical Rayleigh–Ritz method and the independent coordinate coupling method.

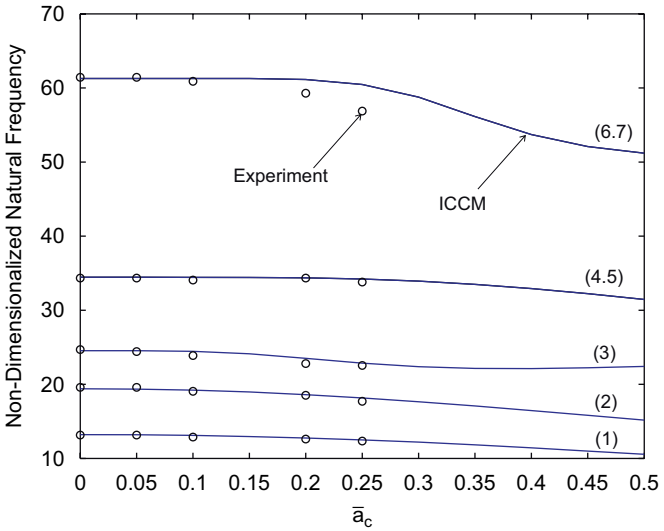

Fig. 10. Non-dimensionalized natural frequency vs. size of hole for free-edge plate.

the ICCM are in good agreement with the experimental results. It can be concluded from Figs. 12–14 that the ICCM is very effective in dealing with a circular hole. Fig. 15 shows the mode shapes of a simply-supported square plate with a circular hole when $\beta = 0.25$.

8. Discussion and conclusions

This study investigated different methods of free vibration analysis of a rectangular plate with a either rectangular or circular hole. The classical Rayleigh–Ritz method (RRM) based on the global coordinate or the finite-element method was presented. The procedure of the classical RRM was first explained in detail. Then, a new method that simplifies the numerical calculations based on the global coordinates attached to the plate and the local coordinates attached to the hole was developed. This method was called the independent coordinate coupling method (ICCM). In applying the classical RRM based on the global coordinates only, the

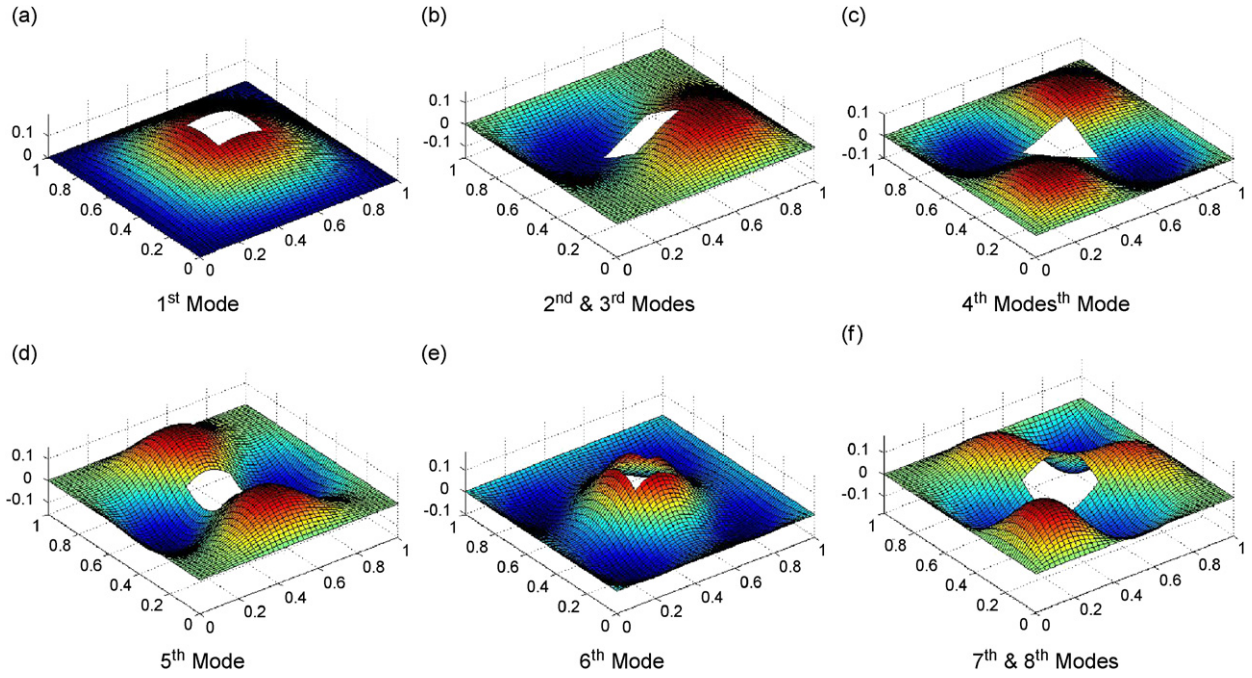

Fig. 11. Mode shapes of simply-supported square plate with a square hole ($\bar{a}_c = 0.2$).

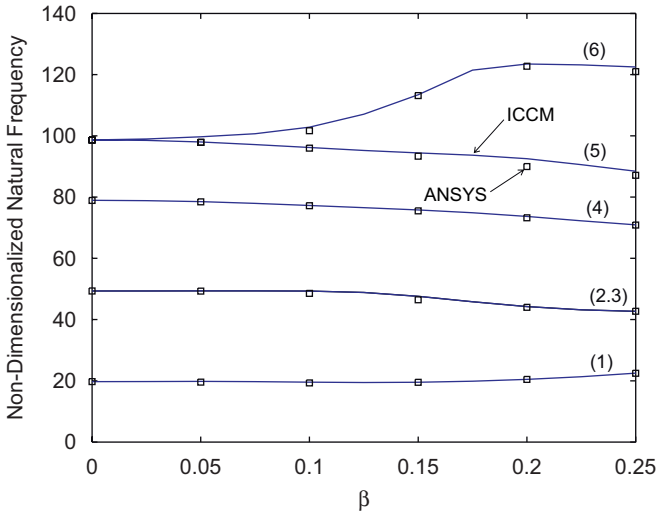

Fig. 12. Simply-supported square plate with a circular hole.

kinetic and potential energies of the rectangular plate with a hole were calculated by subtracting the hole domain in the integrals. For a simply-supported rectangular plate, the exact expressions that reflect the effect of the hole can be derived, although the derivation is very difficult for the clamped and free-edge rectangular plates. Hence, numerical integrations should be used instead, which require considerable amount of computational time. The ICCM developed in this paper employs the local coordinates attached to the hole and the admissible functions expressed in terms of the local coordinates. The expressions for the kinetic and potential energies for the hole domain are then derived. Since the plate inside the hole domain can be regarded as a virtual free-edge plate, the energies, which are to be subtracted from the total energies, can be easily

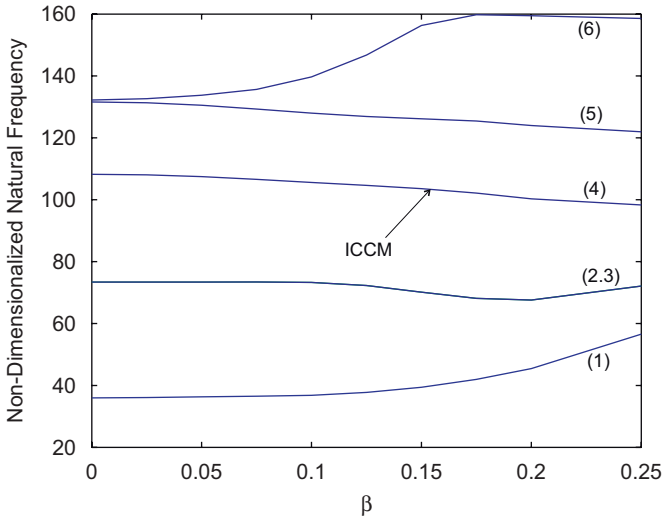

Fig. 13. Clamped square plate with a circular hole.

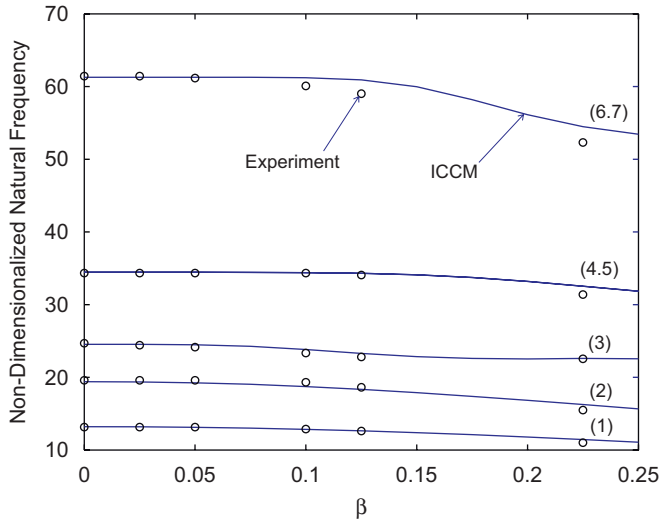

Fig. 14. Free-edge square plate with a circular hole.

expressed in closed form. The resulting total energies are expressed in terms of generalized coordinates, which belong to either global or local coordinates. Hence, we need to unify the generalized coordinates. To this end, the relationship between the generalized coordinates belonging to the local coordinates and the generalized coordinates belonging to the global coordinates was derived using the displacement matching condition inside the hole domain and the orthogonal property of the admissible functions.

To verify results of the proposed ICCM, numerical calculations were carried out using the classical RRM based on the global coordinates only and the commercial finite element program. Experiments were also carried out for the free-edge square plate with a square and circular hole. Both numerical and experimental results showed that good agreement exists between the results by the ICCM and the results obtained by the different algorithms and experiments. Hence, it can be concluded that the proposed ICCM can be effectively used for the free vibration analysis of a rectangular plate with either a rectangular or circular hole.

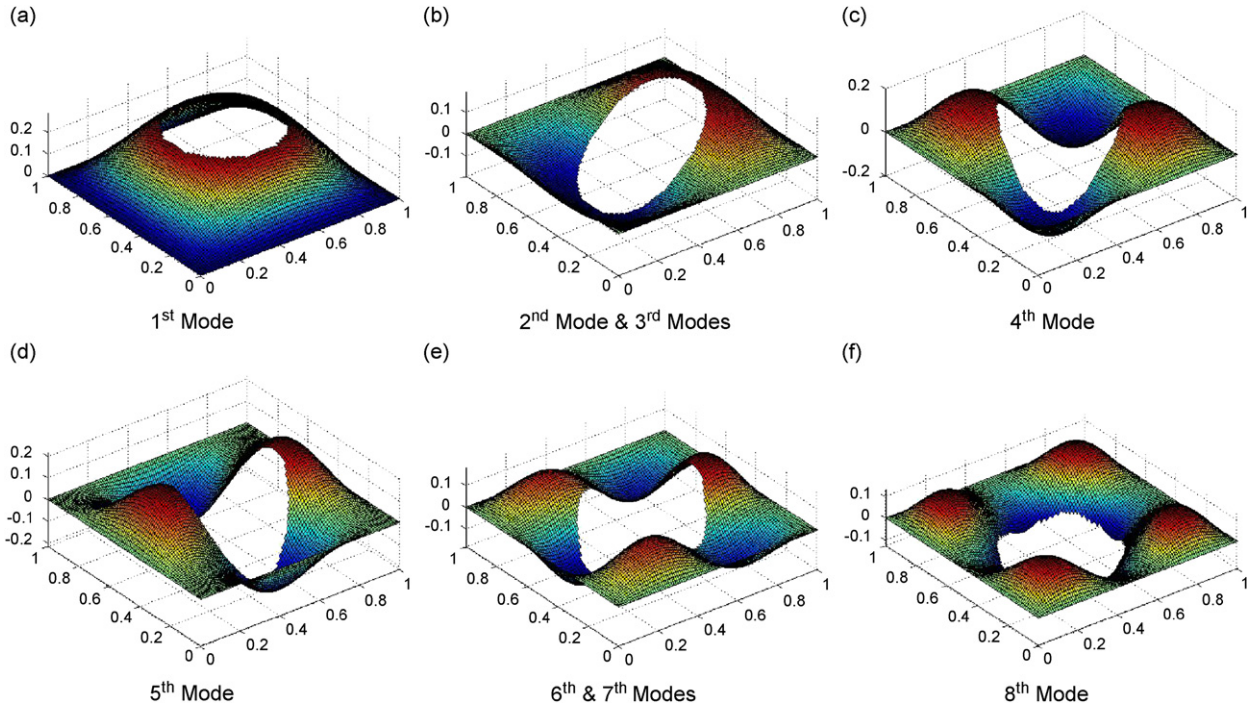

Fig. 15. Mode shapes of simply-supported square plate with a circular hole ($\beta = 0.25$).

Acknowledgement

This research was supported by the Dongguk University Research Fund.

References

[1] L.J. Monahan, P.J. Nemergut, G.E. Maddux, Natural frequencies and mode shapes of plates with interior cut-outs, *The Shock and Vibration Bulletin* 41 (1970) 37–49.
[2] P. Paramasivam, Free vibration of square plates with square opening, *Journal of Sound and Vibration* 30 (1973) 173–178.
[3] G. Aksu, R. Ali, Determination of dynamic characteristics of rectangular plates with cut-outs using a finite difference formulation, *Journal of Sound and Vibration* 44 (1976) 147–158.
[4] A. Rajamani, R. Prabhakaran, Dynamic response of composite plates with cut-outs. Part I: Simply-supported plates, *Journal of Sound and Vibration* 54 (1977) 549–564.
[5] A. Rajamani, R. Prabhakaran, Dynamic response of composite plates with cut-outs. Part II: Clamped–clamped plates, *Journal of Sound and Vibration* 54 (1977) 565–576.
[6] R. Ali, S.J. Atwal, Prediction of natural frequencies of vibration of rectangular plates with rectangular cutouts, *Computers and Structures* 12 (1980) 819–823.
[7] K.Y. Lam, K.C. Hung, S.T. Chow, Vibration analysis of plates with cut-outs by the modified Rayleigh–Ritz method, *Applied Acoustics* 28 (1989) 49–60.
[8] K.Y. Lam, K.C. Hung, Vibration study on plates with stiffened openings using orthogonal polynomials and partitioning method, *Computers and Structures* 37 (1990) 295–301.
[9] R.B. Bhat, Natural frequencies of rectangular plates using characteristic orthogonal polynomials in Rayleigh–Ritz method, *Journal of Sound and Vibration* 102 (1985) 493–499.
[10] R.B. Bhat, Plate deflections using orthogonal polynomials, American Society of Civil Engineers, *Journal of the Engineering Mechanics Division* 111 (1985) 1301–1309.
[11] R.B. Bhat, Numerical experiments on the determination of natural frequencies of transverse vibrations of rectangular plates of nonuniform thickness, *Journal of Sound and Vibration* 138 (1990) 205–219.
[12] P.A.A. Laura, E. Romanelli, R.E. Rossi, Transverse vibrations of simply-supported rectangular plates with rectangular cutouts, *Journal of Sound and Vibration* 202 (2) (1997) 275–283.

[13] T. Sakiyama, M. Huang, H. Matsuda, C. Morita, Free vibration of orthotropic square plates with a square hole, *Journal of Sound and Vibration* 259 (1) (2003) 63–80.
[14] S. Takahashi, Vibration of rectangular plates with circular holes, *Bulletin of JSME* 1 (4) (1958) 380–385.
[15] C.V. Joga-Rao, G. Pickett, Vibrations of plates of irregular shapes and plates with holes, *Journal of the Aeronautical Society of India* 13 (3) (1961) 83–88.
[16] T. Kumai, The flexural vibrations of a square plate with a central circular hole, *Proceedings of the Second Japan National Congress, Applied Mechanics* (1952) 339–342.
[17] R.F. Hegarty, T. Ariman, Elasto-dynamic analysis of rectangular plates with circular holes, *International Journal of Solids and Structures* 11 (1975) 895–906.
[18] F.E. Eastep, F.G. Hemmig, Estimation of fundamental frequency of non-circular plates with free, circular cutouts, *Journal of Sound and Vibration* 56 (2) (1978) 155–165.
[19] K. Nagaya, Transverse vibration of a rectangular plate with an eccentric circular inner boundary, *International Journal of Solids and Structures* 16 (1980) 1007–1016.
[20] H.S. Lee, K.C. Kim, Transverse vibration of rectangular plates having an inner cutout in water, *Journal of the Society of Naval Architects of Korea* 21 (1) (1984) 21–34.
[21] K.C. Kim, S.Y. Han, J.H. Jung, Transverse vibration of stiffened rectangular plates having an inner cutout, *Journal of the Society of Naval Architects of Korea* 24 (3) (1987) 35–42.
[22] K. Itao, S.H. Crandall, Natural modes and natural frequencies of uniform, circular, free-edge plates, *Journal of Applied Mechanics, Transactions of the ASME* 46 (1979) 448–453.